47th SME North American Manufacturing Research Conference, Penn State Behrend Erie, Pennsylvania, 2019

Effect of processing parameters on the microstructure and mechanical behavior of a silicon carbide-silica composite

Damian Beasock, T. Michael Stokes, Ahmed El-Ghannam, Tony Schmitz*

University of North Carolina at Charlotte, Mechanical Engineering and Engineering Science, Charlotte, NC, 28223, USA

* Corresponding author. Tel.: +1 (704) 687-5086; fax: +1 (704) 687-8345. *E-mail address:* tony.schmitz@uncc.edu

Abstract

Silicon carbide (SiC) is an inert material with excellent thermomechanical properties for many optoelectronic, structural, and ballistic applications. However, manufacturing SiC components is challenging due to the high temperatures (> 2000 deg C) and pressures (1000-2000 atm) required for traditional sintering processes. The objective of the present research study is to enable the additive manufacture of SiC components using a new powder bed, sodium hydroxide (NaOH) binder-jetting process. The innovation is the secondary crystal growth (SiO_2) that serves to bridge and close the gaps between the SiC particles via a chemical attack (oxidation) of their surfaces by the NaOH solution. To evaluate the process, SiC powder was mixed with a NaOH-water solution at room temperature and shaped into 10 mm diameter by 15 mm long cylinders in a mold with compaction by hand pressure only. This approach was implemented to simplify testing while still mimicking the eventual powder bed, binder-jetting process where moderate pressure is applied by the roller from one powder layer to the next. Samples were thermally treated at moderate temperatures (approximately 1000 deg C) for a few hours. As the thermal treatment temperature and duration increased, the density also increased. In conjunction with the increase in density, the compressive strength increased. Scanning electron microscopy results are presented to validate the formation of secondary crystal growth.

Keywords: Additive manufacturing, silicon carbide, powder bed, sodium hydroxide

1. Introduction

Silicon carbide (SiC) offers high elastic modulus, low density, low coefficient of thermal expansion (CTE), and high thermal conductivity. This makes it an ideal material candidate for many demanding applications. These include, for example:

- lightweight mirrors and structural components for ground- and space-based imaging systems, such as telescopes and satellites – The ability to match materials between the mirrors and support structure is ideal because issues with mismatched CTEs and the corresponding thermal distortion caused by temperature variations and gradients are minimized.

- lithography positioning tools/stepper systems – The ability to integrate threaded inserts, mounting locations, and the wafer chuck with the stage mirrors offers significant design freedom and enhanced performance.
- scanning mirror systems [1] – The integration of lightweight, stiff mirrors with gimbal attachments and other structural features again provides design freedom as well as assembly and alignment cost reductions.
- ballistic protection [2] – The ability to 3D print near-net shape geometries will increase design freedom and reduce production cost and time for improved protection against ballistic threats. Applications include both vehicle and body armor (e.g., 3D scan a soldier's geometry and use on-demand printing to produce customized protective plates).

While SiC offers desirable material properties, the difficulty in its manufacture currently limits the application opportunities. In space-based optics fabrication (see Fig. 1), for example, "although SiC appears to be an ideal optical material from a material properties standpoint, the cost and lead-time associated with the preliminary shaping, lightweighting, and optical finishing… have been major impediments to the widespread use of the material in optical systems" [4].

Fig 1. Example SiC optics for space applications [3]. The areal density is reduced by honeycomb lightweighting.

Manufacturing process options currently include:
1. Hot pressed SiC – in this process micrometer-scale alpha phase SiC particles are consolidated in a mold at high temperatures (> 2000 deg C) and pressures (1000-2000 atm) to form simple shapes. Sintering aids and grain growth inhibitors are used to increase the density. Grinding or diamond machining is then used to produce the final geometry and polishing and lapping are used to generate the final surfaces. Because the material removal rates are low in SiC (< 5% of the rates for glasses and metals [4]) due to its high hardness and strength, the secondary processing steps are time-consuming and costly [5].
2. CVD SiC – an organo-metallic vapor is deposited onto a heated substrate (> 1300 deg C). This gives a beta (cubic) phase SiC coating with fine columnar grains. It is typically used as a thin layer on top of an existing structure (e.g., graphite or SiC) to encapsulate the surface [4-5].
3. Reaction bonded SiC – a SiC alpha (hexagonal) phase slurry is slip cast (injected) into a mold with the negative of the desired geometry. This green part is removed from the mold and, if required, it can be machined to modify the geometry. The part is then heated to sinter the SiC particles. This structure has an open porosity which is filled with free silicon in a second heating operation (i.e., reaction bonding). This final microstructure offers a uniform dispersion of Si and SiC regions and is typically finish machined to produce the desired part. Reaction bonding produces near-net shapes and, therefore, offers

reduced machining time, but at the cost of a mold which can be expensive for low-volume production [5-7].
4. Graphite conversion – POCO Graphite offers a graphite preform, SUPERSiC, which can be machined to a near-net shape. The graphite is then purified and subjected to a proprietary conversion process which substitutes silicon atoms for carbon atoms to obtain SiC [8]. This conversion process is limited to a 3 mm depth (6 mm total thickness) and the final part is typically CVD coated to improve the optical finishing properties [5].

In addition to these "traditional" manufacturing processes, additive manufacturing was recently tested for alumina (or aluminum oxide, Al_2O_3) parts [9]. In this study, the performance of sintered alumina was compared to 3D printed alumina specimens for ballistic protection, where the ultimate application is customized armor for soldiers, vehicles, and equipment. Pressurized spray deposition of a proprietary blend of ceramic powder and a polymeric binder was applied layer-by-layer to produce the 3D printed samples. After printing, sintering was completed to remove the polymer; this naturally caused significant shrinkage due to the polymer loss and added the requirement for post-process grinding to achieve tight dimensional tolerances. However, testing demonstrated that the sintered alumina was only 13% more effective against ballistic penetration than the 3D printed alumina specimens. This promising result suggests that additional ceramic 3D printing research is warranted in the field of ballistic protection.

The new method employed in this study differs from prior processes and research. Rather than relying on: 1) high temperatures and pressures within a mold; or 2) a polymer binder that serves as the preliminary support structure until it is removed by sintering, the new approach is based on a chemical attack (oxidation) of the SiC powder surface using a NaOH-water binder. This produces an amorphous silica layer on the SiC surface that enables the growth of secondary SiO_2 crystals at elevated temperatures. These secondary crystals bridge the gaps between the adjacent SiC grains and serve to strengthen and increase the density of the final part.

2. Materials and Methods

The innovation in this research is oxidation and crystal growth on the surface of SiC grains using an NaOH-water binder. The process chemistry, where the NaOH binder facilitates the release of free silanol groups on the SiC surface that spontaneously re-polymerize to form amorphous SiO_2 (silica), is described in the following paragraphs.

The bond between Si and C in SiC prior to any chemical modification is directional. Because the electronegativity of Si is lower (1.8) than that of C (2.5), the electron cloud shifts toward C and produces a polarized bond, where the Si is positive and the C is negative.

$$Si^{\delta+} - C^{\delta-} \tag{1}$$
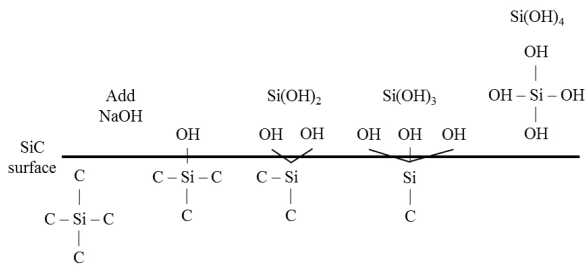
Fig. 2. Formation of amorphous SiO_2 (silica) gel layer on the SiC surface.

The oxidation step is initiated by the addition of the NaOH to the SiC surface. The use of the ionized NaOH binder results in the preferable oxidation of the Si. Specifically, the negatively charged OH preferentially bonds to the positively charged Si. An atomic level representation of the oxidation reaction is:

$$\left(Si^{\delta+}-C^{\delta-}\right)+{}^{\delta-}OH \rightarrow \left(\equiv Si-OH\right)+\left(H-C\equiv\right), \text{ (2)}$$
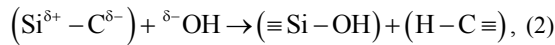
where $\equiv$ indicates three additional bonds and $^-$ represents a single bond. Figure 2 displays the oxidation species that are produced as the NaOH solution opens the original SiC bonds. These species include: $Si(OH)_2$, $Si(OH)_3$, and $Si(OH)_4$. The $Si(OH)_4$, silanol, groups are made possible by the diffusion of Si across the original SiC surface.

There is thermodynamic motivation for the silanol groups to re-polymerize at room temperature and produce the highly porous SiO_2 (silica) gel layer. This includes the removal of water from adjacent OH bonds to form the amorphous silica gel. The structural characteristics of the silica gel layer that forms on the SiC (particle) surfaces include an amorphous SiO_2 a disordered lattice of Si^{4+} and O^{2-} with high porosity and surface area. The negative charge of the $Si-O^-$ is balanced by H^+ to form $Si-OH$ "dangling" bonds.

These physicochemical characteristics of the silica gel layer facilitate its crystallization when heat is added. The presence of the Na ions promotes the nucleation of crystalline SiO_2 that continues to grow on the SiC surface. In addition, the Na ions are network modifiers that increase the release and mobility of the silicate ions during crystal growth. Finally, the gel porosity enables oxygen diffusion towards the SiC surface, which creates more SiO_2 for crystal growth. The result is depicted in Fig. 3.
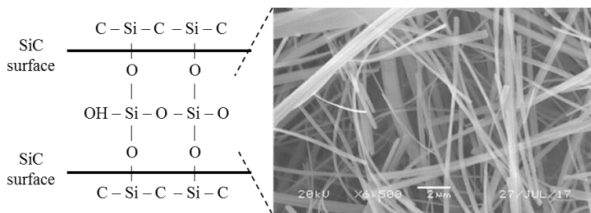
Fig. 3. The addition of heat promotes crystallization of the SiO_2 gel layer. The crystal growth serves to connect the adjacent surfaces (grains). The inset shows an example SEM image of the crystal growth between grains (not shown) after heating.

3. Experimental approach

The effect of the NaOH concentration and thermal treatment on the structure and properties of the material was studied. For all samples, 3000 mg of SiC 40 µm diameter powder was mixed with 6.25% by mass (200 mg) nanopowder (<80 nm APS). SiC powders were purchased from US Nanomaterials, Inc.

3.1 Effect of NaOH concentration

Sodium hydroxide ACS reagent pellets were purchased from Sigma Aldrich. Sodium hydroxide solutions of variable concentrations (5%, 10%, 15%, 20%, 40% NaOH by weight) were prepared with nano pure water from a Barstead Easypure RoDi water purifier. The SiC powder was mixed separately with 500 µL of NaOH solution and formed into a 10 mm diameter cylindrical sample using a pellet die. Only minimal hand pressure was applied to form samples. Sample height was between 23 mm and 26 mm. These samples were left to dry in the open air at ambient temperature for 24 hours and were then subjected to thermal treatment at 900 deg C for 2 hrs.

3.2 Effect of thermal treatment parameters

Samples were heat treated in an air atmosphere at varying temperatures {800, 900, 1000, 1100, 1200} deg C for 2 hrs using a Thermolyne Benchtop Furnace. All ramp segments used a rate of 1 deg C/min. All samples were ramped to 100 deg C, held at 5 hrs to remove any humidity, ramped to 350 deg C, held at 6 hrs to remove any impurities in the silica gel. The temperature was finally ramped to the final sintering temperature. The samples were left in the closed furnace to return to room temperature after sintering.

3.3 SEM-EDX morphology analysis

To study the microstructure, SEM-EDX analysis was performed on the fracture surface of samples used for mechanical tests. A JEOL 6480 Scanning Electron Microscope was used to analyze particle fusion, grain boundary, porosity, and crystal growth. Elemental composition of the microstructure features were characterized by EDX using an Oxford Instruments INCA EDS in combination with the JEOL 6480 SEM.

3.4 X-Ray diffraction analysis

XRD was used to determine the crystal structure of each phase in the composite. A PANalytical X'Pert Pro/MRD was used for all scans. Samples were ground to a powder with a pestle and mortar. The powder was adhered to a silicon zero background disk with double-sided tape. The scanning X-ray beam was Ni filtered Cu K alpha radiation with wavelength of 1.541874 Angstroms. Radiation was produced at 45 kV and 40 mA. Incident beam optics included a 1/2 degree divergence slit and a 0.02 mm nickel filter. The diffracted beam optics included a parallel plate collimator slit and 0.04 radian soller slit. Scan time step was 1.0 sec and the 2θ range was from 20° to 40°.

3.5 Density measurement

Density was calculated from the measured sample volume and sample mass. Five (n = 5) replicate samples were used for each set of density samples. The dimensions of the cylindrical samples were measured using a digital caliper and the mass was measured using an analytical balance.

3.6 Mechanical testing

Heat treated samples were compression tested until failure using an Instron 5582. Samples were compressed at a rate of 2 mm/min until failure. Five replicate samples were used for each NaOH solution concentration and each heat treatment temperature. Strength was taken as the highest measured force divided by the cross sectional area of the sample. Young's modulus was taken as the slope of a linear portion of the stress-strain plot.

3.7 Statistical analysis

All mechanical tests were completed using five replicates and the results are presented as mean +/- the standard deviation. The errors bars represent the standard deviation. P values were calculated using Student's T-test and P < 0.05 was considered statistically significant.
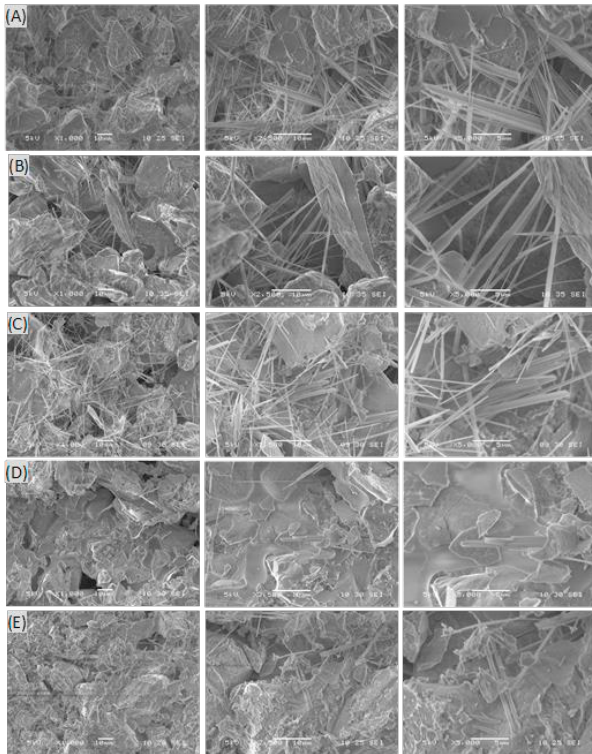
Fig 4. SEM images of fracture surfaces for samples prepared with different NaOH concentrations. (A) 5% NaOH, 900 degC/2 hr. (B) 10% NaOH, 900 deg C/2 hr. (C) 15% NaOH, 900 deg C/2 hr. (D) 20% NaOH, 900 deg C/2 hr. (E) 40% NaOH, 900 deg C/2 hr.
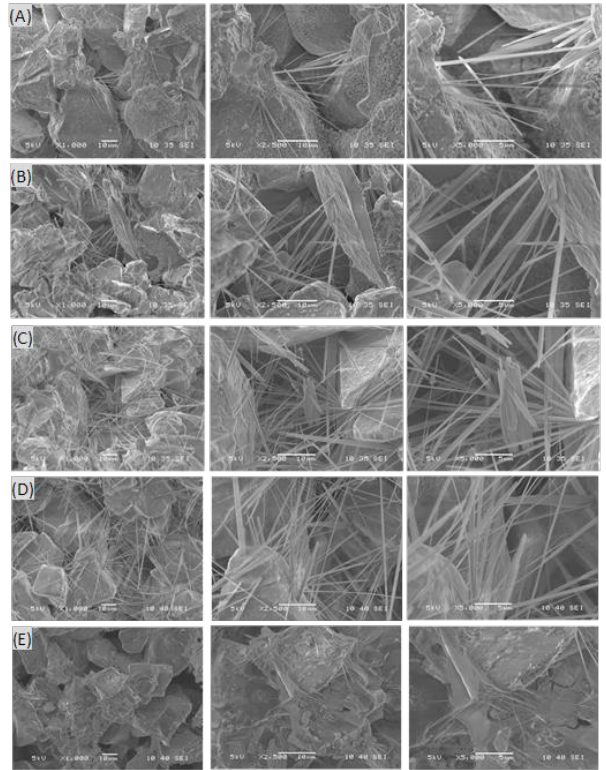
Fig 5. SEM micrographs showing morphology of crystal growth for samples prepared at different temperatures. (A) 800 deg C/2 hr. (B) 900 deg C/2 hr. (C) 1000 deg C/2 hr. (D) 1100 deg C/2 hr. (E) 1200 deg C/2 hr.

4. Results

4.1. SEM-EDX morphology analysis

SEM observations showed that increasing the NaOH concentration up to 20% leads to an increase in grown crystal density. Samples treated with 40% NaOH exhibited less crystal growth, but with more silica in the form of a smooth layer on the SiC particles; see Fig. 4.

Samples treated at 800 deg C/2 hr showed the most crystal growth. Samples treated at 900 deg C/2 hr and 1000 deg C/2 hr show similar crystal density; see Fig. 5.

Samples treated at 1100 deg C/2 hr and 1200 deg C/2 hr exhibited some melting of crystals, lower density of crystals, and more filling of the grain boundary; see Fig. 5E. Lower temperatures (800 deg C) appeared to favor crystal growth. Higher temperatures (1100 deg C and above) showed melting of the crystals with a denser overall matrix.

4.2. X-Ray diffraction analysis

XRD data showed that while changing NaOH concentration, samples had varying ratios of cristobalite to quartz signals; see Table 1. As the NaOH concentration increased, quartz intensity reduced and cristobalite intensity increased; see Fig. 6. XRD data revealed that changing heat treatment temperature produced three silica phases. One consistent SiC phase is observed in all samples. The SiC

phase was present as SiC 6H and the SiO_2 was found as quartz, cristobalite, and tridymite. At 800 deg C quartz was the only silica phase. Both quartz and cristobalite were present at 900 deg C. Cristobalite is the only phase present at 1000 deg C. At both 1100 deg C and 1200 deg C, tridymite was present. The cristobalite peak at 21.8° overlapped with the 21.6° peak for tridymite; see Fig. 7.

Table 1. Relative peak intensity of cristobalite to quartz in samples prepared with different NaOH concentrations.

NaOH concentration	Cristobalite to quartz signal
5% NaOH	140%
10% NaOH	180%
15% NaOH	250%
20% NaOH	771%
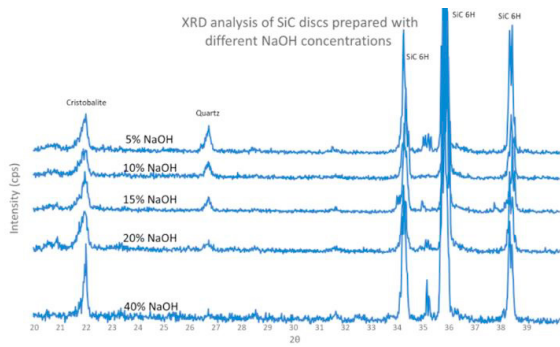
Fig 6. XRD spectra of samples treated with various NaOH concentrations.
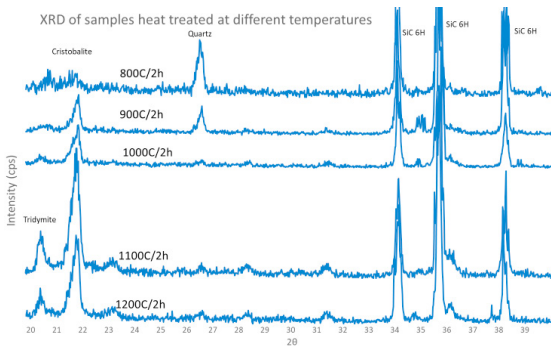
Fig 7. XRD spectra for samples prepared at different temperatures. The quartz peak is found at 26.6. Cristobalite signal is found at 21.8. Tridymite signal is found at 21.6 and 20.5.

4.3. Density measurements

Density data shows no significant change in density among samples pretreated with various NaOH concentrations from 5% to 20%. The density was 1.7 g/cm^3 for samples treated with 5%, 10%, and 20% NaOH. On the other hand, samples treated with 40% NaOH expanded in volume and exhibited a decrease in density to 1.5 g/cm^3 (Fig. 8). There was a steady mass increase after heat treatment from 5% to 40% NaOH. With changing heat treatment temperature,

density showed an increase up to 1100 deg C/2 hr. There was a significant change in density when comparing the 800 deg C/2 hr protocol to the 1100 deg C/2 hr protocol ($P < 0.001$); see Fig. 9.
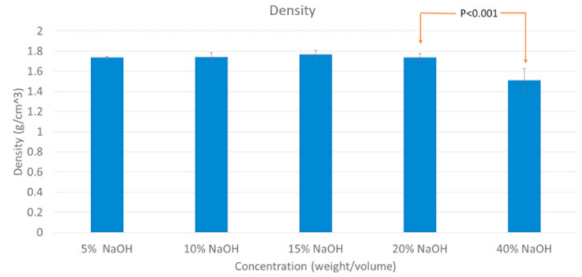
Fig 8. Density of samples treated with different concentrations of NaOH.
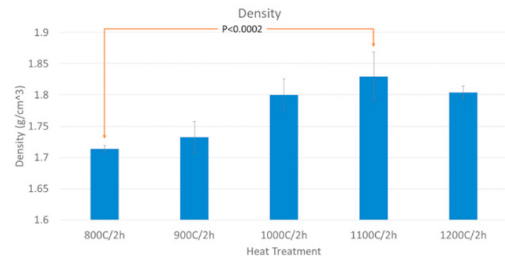
Fig 9. Density for samples made with varying heat treatments.

4.4. Mechanical testing

The compression strength and modulus of elasticity increased from 30 MPa to 78 MPa and from 6 GPa to 9 GPa as the concentration of the NaOH used for surface modification increased from 5% to 20%; see Fig. 10. Samples treated with 40% NaOH acquired strength and elasticity lower than that treated with 20% NaOH. ($P < 0.0008$).

Compression data for different heat treatment temperatures show a peak in mechanical properties at 1000 deg C for strength, toughness, and modulus. As the temperature increased from 900 deg C to 1000 deg C, compression strength and modulus increased from 58 MPa to 91 MPa ($P < 0.002$) and from 9 GPa to 12 GPa ($P < 0.04$); see Fig 11.

5. Discussion

By varying the concentration of the starting NaOH solution and the heat treatment temperature, the microstructure was controlled and exhibited consistent mechanical properties that were dependent on the observed microstructure. NaOH was used to corrode the surface of the SiC particles to form a silica gel layer. Secondary crystal growth occurred from this layer during heat treatment. Quantification of cristobalite after treatment with various concentrations of NaOH showed that as the concertation of NaOH increased from {10 to 20} weight

%, the cristobalite content in the SiC samples increased from {4.5 to 8.5} weight % after treatment at 900 deg C/2 hr; see Fig 12. The silica crystals enhanced connectivity between the SiC particles and contributed to an increase in the mechanical strength (Fig.5). Interestingly, it was observed that the NaOH concentration had an effect on the phase transformation of silica. At 5% NaOH, a mixture of cristobalite and quartz formed after treatment at 900 deg C/2 hr. As the NaOH concentration increased up to 40%, the quartz peaks disappeared and the dominant phase became cristobalite. The transformation of quartz to cristobalite was enhanced by the presence of the Na ions, which acted as impurities in the silica phase.

Typically, cristobalite and tridymite form at 867 deg C to 1470 deg C and 1470 deg C to 1727 deg C, respectively [11]. Previous studies also report using alkali species as a flux to attain these silica phases at temperatures of 700 deg C to 1350 deg C [10, 11]. These temperatures are within the ranges of the heat treatments completed in the present study. Therefore, it is likely that the presence of NaOH not only forms the silica layer, but also reduces the required temperature to achieve the observed silica phases.
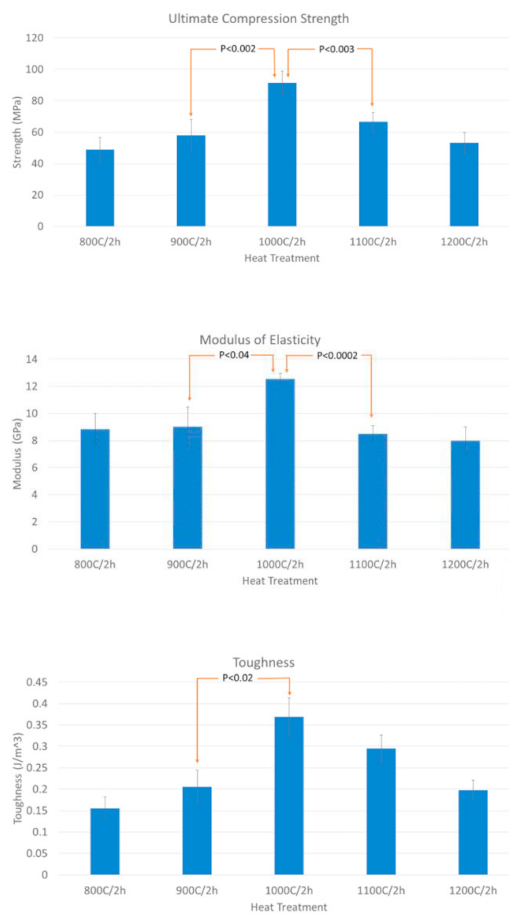
Fig 11. Mechanical properties of samples heat treated at different temperatures.

Fig 10. Mechanical properties of samples with varying concentrations of NaOH solution.

Data in the literature have described the role of alkali ions in the transformation of quartz to cristobalite. Shinohara et al. showed that heating husk ash containing 92.95% silica and close to 5% alkali ions resulted in the formation of cristobalite at 1000 deg C and partial transformation of cristobalite to tridymite at 1100 deg C [13]. In a separate study, the transformation temperature of quartz to cristobalite and tridymite was significantly reduced to 900 deg C/17 hr. These studies indicate that the higher the percent of alkali ions in the silica, the lower the temperature for phase transformation.

It should be noted that in the previous studies [11, 13] the concentration of the alkali oxides were significantly higher than the 1% Na_2O incorporated in the silica phase in the SiC-SiO_2 composite samples prepared with 10% NaOH here. Increasing the Na_2O from 1% to 4% in SiC resulted in domination of cristobalite as the only silica phase in the material. In association with the direct crystallization of the silica gel to cristobalite SEM showed a nearly complete absence of the needle-like secondary crystal growth. Therefore, the secondary crystals growth is dependent on the presence of quartz. In addition to the effect of Na_2O content, it was observed that increasing the thermal treatment

temperature decreased the quartz content and facilitated phase transformation to cristobalite. SEM showed the most extensive secondary crystal growth to be in samples treated at 800 deg C and XRD showed these crystals to be quartz.
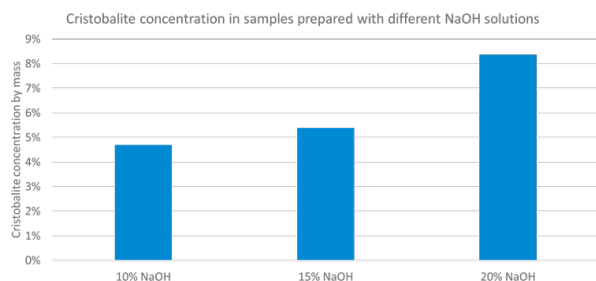
Fig 12. Percent weight of cristobalite in samples made with varying NaOH concentrations.

The strength and modulus of quartz are higher than cristobalite [12]. A correlation was observed between the increased strength and the increase in cristobalite XRD signal. This is seen at temperatures between 800 deg C and 1000 deg C, where mechanical properties increased while the cristobalite to quartz signal ratio increased. Even though samples treated at 800 deg C showed denser crystal growth, these samples also showed a low cristobalite signal and high quartz signal and had low mechanical properties. Since the morphology of crystals changed at higher temperatures while forming tridymite, it cannot be concluded if increased presence of tridymite would change mechanical properties. Samples treated at 1000 deg C for 2 hr showed the highest mechanical properties. This is due to the presence of cristobalite secondary growth crystals.

The study results suggest that the silica phase morphology contributed significantly to the mechanical properties of the material. Similar crystal morphology was seen at temperatures up to 1000 deg C. Raising the treatment temperature to 1100 deg C resulted in melting of the secondary growth crystals. Scanning electron micrographs (Figs. 5D and 5E) show melted crystals laying across grain surfaces rather than growing outward. This lack of outward crystal growth reduced particle connectivity and diminished material strength. This is seen in the compression strength data (Figs. 10 and 11).

Although pre-treatment of SiC with 40 % NaOH increased the silica content, the SEM showed the silica phase to be in the form of a coating layer rather than needle shaped crystals that connect the SiC particles together. In conjunction with the absence of secondary growth crystals, there was a significant decrease in the mechanical properties. The decrease in the mechanical properties can be attributed to the decrease in the percent SiC as the percent silica phase increases. Fracture surface analysis showed the samples to be more porous with occasional micro cracks in the silica phase in between the particles. Therefore, the fracture mechanism seems to be initiated by the defects in the silica phase.

References

[1] http://www.laserfocusworld.com/articles/print/volume-44/issue-4/features/optical-materials-silicon-carbide-mirrors-benefit-high-speed-laser-scanning.html.
[2] http://ceramics.org/wp-content/bulletin/2017/JanFeb2017/janfeb17.html#p=38.
[3] https://www.coorstek.com/english/solutions/industries/transportation/aerospace/optics-imaging/.
[4] Johnson, J.S., Grobsky, K.D., and Bray, D., 2002, Rapid fabrication of lightweight silicon-carbide mirrors, International Symposium on Optical Science and Technology, pp. 243-253.
[5] Tobin, E., Magida, M.B., Kishner, S.J., and Krim, M.H., 1995, Design, fabrication, and test of a meter-class reaction bonded SiC mirror blank, SPIE 1995 International Symposium on Optical Science, Engineering, and Instrumentation, pp. 12-21.
[6] Robichaud, J., Schwartz, J., Landry, D., Glenn, W., Rider, B., and Chung, M., 2005, Recent advances in reaction bonded silicon carbide optics and optical systems, Optics & Photonics, pp. 586802-586802.
[7] Robichaud, J.L., 2003, SiC optics for EUV, UV, and visible space missions, Astronomical Telescopes and Instrumentation, pp. 39-49, International Society for Optics and Photonics.
[8] http://poco.com/IndustriesApplications/Industrial/Optics.aspx.
[9] http://ceramics.org/wp-content/bulletin/2017/JanFeb2017/janfeb17.html#p=38.
[10] Eitel, W., 1957, Structural anomalies in tridymite and cristobalite, Am Ceram Soc Bull, 36, pp. 142-148.
[11] Shinohara, et al., 2004, Quantitative analysis of tridymite and cristobalite crystallized in rice husk ash by heating. Industrial Health, 42, pp. 277-285.
[12] Willi Pabst, E.G., 2013, Elastic properties of silica polymorphs – A review, Ceramics.
[13] Holmquist, S.B., 1961, Conversion of quartz to tridymite, American Ceramic Society, 44(2), pp. 82-86.